Interacting Weighted Ensemble Kalman Filter applied to Underwater Terrain Aided Navigation

Camille Palmier, Karim Dahia, Nicolas Merlinge, Dann Laneuville, Pierre del Moral

Interacting Weighted Ensemble Kalman Filter applied to Underwater Terrain Aided Navigation

Camille Palmier[1], Karim Dahia[2], Nicolas Merlinge[3],
Dann Laneuville[4] and Pierre Del Moral[5]

***Abstract*— Terrain Aided Navigation (TAN) provides a drift-free navigation approach for Unmanned Underwater Vehicles. This paper focuses on an improved version of the Weighted Ensemble Kalman Filter (WEnKF) to solve the TAN problem. We analyze some theoretical limitations of the WEnKF and derive an improved version which ensures that the asymptotic variance of weights remains bounded. This improvement results in an enhanced robustness to nonlinearities in practice. Numerical results are presented and the robustness is demonstrated with respect to conventional WEnKF, yielding twice as less non-convergence cases.**

I. Introduction

Nonlinear state estimation is a challenging issue when measurements yield state multimodality, i.e. to a given measurement may correspond several solutions in the state space. For example, state multimodality occurs in the case of Terrain Aided Navigation (TAN [1], [2]). TAN is a commonly employed method in autonomous vehicles navigation which is a broad and extensive field of study. Autonomous/Unmanned underwater vehicle (AUV/UUV) navigation is often based on Inertial Navigation Systems (INS) measurements [3]. Although INS are autonomous and reliable, they provide imperfect measurements (e.g. subject to bias, noise) that result in a drifting error in the navigation solution. To correct the navigation drift, INS can be combined with a TAN method.TAN provides a drift-free navigation tool which is a powerful alternative to current navigation methods that include exogenous measurements (e.g. GPS). Resurfacing for GPS is possible but is often excluded for discretion purposes and also because it can easily be jammed. This is especially true for military-grade UUVs. TAN aims to retrieve the vehicle's current state (e.g. position, velocity) by matching a terrain profile obtained from a sensor with a profile reconstructed from an embedded map of the operation area. This paper addresses the multi-beam telemeter based TAN for UUVs. The multi-beam telemeter provides a series of depth measurements along the trajectory. If the terrain contains sufficient information, this kind of sensor is able to retrieve the position.

Performing INS/TAN fusion makes it necessary to resort to nonlinear filtering algorithms. In the presence of strong nonlinearities and multimodality due to terrain map ambiguities, the Extended Kalman Filter (EKF [4]) is known to be unreliable. The linearization of terrain areas where abrupt changes in seabed elevation occur generates numerical instabilities that may result in estimation divergence. In order to avoid linearization, several stochastic filters were proposed such as the Particle Filter (a.k.a. Monte Carlo methods [5]) and the Weighted Ensemble Kalman Filter [6].

Sequential Monte Carlo methods rely on weighted sampling, based on a proposal density. In general, the proposal density is difficult to compute for a given problem. If the proposal density is taken equal to the prior density, the Monte Carlo errors can be significant due to an insufficient recovery between the supports of the prior and the likelihood densities. In this case, the filter may diverge. On the contrary, if the proposal density is close to the posterior density, then the filter remains theoretically stable [7]. Thus, an appropriate choice of the proposal density makes it possible to design more stable filters.

This paper focuses on the Weighted Ensemble Kalman Filter (WEnKF), which can be interpreted as a particle filter [6]. WEnKF consists of determining a Gaussian proposal density using a Kalman Filter on each sample before updating the sample weights. This method helps the proposal density to approach the posterior density. However, in some cases, the obtained proposal density is still not close enough to the posterior density and thus the filter may diverge. To tackle this issue, it is possible to empirically enlarge the support of the proposal density so that it contains the support of the posterior density. In the case of WEnKF, the proposal density is Gaussian. The covariance matrix of the proposal density can be replaced by a sightly larger one (inflation methods, see [7]).

In this paper, an analytic approach is introduced to compute an optimized formulation of the proposal density covariance matrix in terms of weight variance. Indeed, the method consists of choosing the proposal covariance matrix so that it guarantees a finite variance of the weights. In particular, we show that:

- The asymptotic variance of the unnormalized weights admits a finite upper bound if and only if the proposal covariance matrix verifies some assumptions;

This work was developed as part of an agreement between ONERA, Naval Group, INRIA and Bordeaux University.

[1]Camille Palmier is a PhD student at DTIS, ONERA, Palaiseau, France camille.palmier@onera.fr

[2]Karim Dahia is a research scientist at DTIS, ONERA, Palaiseau, France karim.dahia@onera.fr

[3]Nicolas Merlinge is a research scientist at DTIS, ONERA, Palaiseau, France nicolas.merlinge@onera.fr

[4]Dann Laneuville is a senior expert in Information Processing Systems Algorithms, Naval Group, Bouguenais, France dann.laneuville@naval-group.com

[5]Pierre Del Moral is research director at INRIA, Bordeaux Research Center, University of Bordeaux, Talence, France pierre.del-moral@inria.fr

- A proposal covariance matrix can be computed for the WEnKF so that it satisfies these assumptions.

This approach leads to a new version of the WEnKF called Interacting Weighted Ensemble Kalman Filter (IWEnKF).

The paper is organized as follows. Section II recalls the estimation problem formulation and the WEnKF equations. In Section III, the IWEnKF algorithm is introduced and theoretical proofs are provided. Section IV illustrates the performance of the proposed method applied to an underwater TAN example. Section V concludes the paper.

II. Problem statement

We consider the following discrete-time state-space model with hidden states $\{x_k\}_{k\geq 0}$ and observations $\{y_k\}_{k\geq 1}$, taking values in $\mathbb{R}^d$ and $\mathbb{R}^{d_m}$ respectively. The state sequence $\{x_k\}_{k\geq 0}$ is defined as an inhomogeneous Markov chain with initial probability density p_0. $\{x_k\}_{k\geq 0}$ is defined by the following equation:

$$x_k = f_k(x_{k-1}) + \eta_k \tag{1}$$

where f_k is the state function and η_k the process noise. The measurements sequence $\{y_k\}_{k\geq 1}$ is related to the state sequence by:

$$y_k = h_k(x_k) + v_k \tag{2}$$

where h_k is the observation function and v_k the measurement noise. η_k and v_k are independent and identically distributed (i.i.d.), mutually independent and independent of x_0. We will assume that h_k is a nonlinear function.

A. Filtering framework

Bayesian filters aim to estimate the *a posteriori* density of the state variables at the time k given the past measurements. The posterior density will be denoted $p_k(x_k) \triangleq p(x_k|y_{1:k})$ where $y_{i:k} = \{y_i, y_{i+1}, \ldots, y_k\}$ is the vector of all the data y accumulated from time i up to k. The prior density will be denoted $p_{k|k-1}(x_k) \triangleq p(x_k|y_{1:k-1})$. State estimation consists of two steps: prediction and correction.

- The prediction step determines a prior density $p_{k|k-1}(x_k)$ with respect to the transition density $p(x_k|x_{k-1})$ and the previous posterior density $p_{k-1}(x_{k-1})$ via the Chapman-Kolmogorov equation:

$$p_{k|k-1}(x_k) = \int p(x_k|x_{k-1})\ p_{k-1}(x_{k-1})dx_{k-1} \tag{3}$$

- The correction step determines the posterior density of the state with respect to the prior density (3) and the likelihood $g_k(x_k) \triangleq p(y_k|x_k)$. From Bayes' law, one obtains:

$$p_k(x_k) = \frac{g_k(x_k)\ p_{k|k-1}(x_k)}{\int g_k(x_k)\ p_{k|k-1}(x_k)dx_k} \tag{4}$$

If the state and the observation functions are linear, the process and measurements noises are Gaussian, and the initial density p_0 is Gaussian then the Kalman filter provides an optimal analytic iterative formulation of the filtering distribution. The Kalman formulation was extended to nonlinear models, but it is not robust to severe nonlinearities and non-Gaussian densities. For highly nonlinear models, several Monte Carlo methods were proposed to approximate the posterior density.

B. Weighted Ensemble Kalman Filter

The Weighted Ensemble Kalman Filter (WEnKF, [6]) combines the advantages of the Ensemble Kalman Filter and the Particle Filter. Indeed, WEnKF can be used without linear or Gaussian assumptions on the model and was demonstrated to require less particle samples to converge than conventional Monte Carlo methods. The equations of WEnKF are generally presented when the measurement dynamic is linear [6]. A more general version is presented here for the nonlinear case. WEnKF can be interpreted as a particle filter [6] in the meaning that the approximation of the posterior density can be written as a weighted sum of Dirac measures:

$$p_k(x_k) \approx \sum_{i=1}^{N} w_k^i \delta_{x_k^i}(x_k) \tag{5}$$

where N is the number of state samples called particles, $(x_k^i)_{i=1,\ldots,N}$ are the particles, $(w_k^i)_{i=1,\ldots,N}$ are the associated importance weights such that $\sum_{i=1}^{N} w_k^i = 1$ and δ the Dirac delta function centered at 0 such that $\delta_a(x) = \delta_{x-a}$.

WEnKF is composed of three steps:

- Prediction: the particles are drawn from the following proposal density:

$$x_k^i \sim q_k(x_k|x_{k-1}^i, y_k) = \mathcal{N}(x_k; \bar{\mu}_k^i, \hat{P}_k) \tag{6}$$

The mean $\bar{\mu}_k^i$ and covariance matrix $\hat{P}_k$ are computed as follows:

$$\bar{\mu}_k^i = f_k(x_{k-1}^{f,i}) + \hat{K}_k(y_k - h_k(f_k(x_{k-1}^{f,i}))) \tag{7}$$

$$\hat{P}_k = \tilde{P}_k - \hat{K}_k P_Y \hat{K}_k^\top \tag{8}$$

The Ensemble Kalman gain is approximated by:

$$\hat{K}_k = P_{XY} P_Y^{-1} \tag{9}$$

where $\forall\ i = 1, \ldots, N$:

$$x_k^{f,i} = f_k(x_{k-1}^{f,i}) + \eta_k^i \quad \text{and} \quad \tilde{x}_k = \sum_{i=1}^{N} w_{k-1}^i\ x_k^{f,i} \tag{10}$$

$$y_k^i = h_k(x_k^{f,i}) \quad \text{and} \quad \tilde{y}_k = \sum_{i=1}^{N} w_{k-1}^i y_k^i \tag{11}$$

$$\tilde{P}_k = \sum_{i=1}^{N} w_{k-1}^i (x_k^{f,i} - \tilde{x}_k)(x_k^{f,i} - \tilde{x}_k)^\top \tag{12}$$

$$P_Y = \sum_{i=1}^{N} w_{k-1}^i (y_k^i - \tilde{y}_k)(y_k^i - \tilde{y}_k)^\top + R_k \tag{13}$$

$$P_{XY} = \sum_{i=1}^{N} w_{k-1}^i (x_k^{f,i} - \tilde{x}_k)(y_k^i - \tilde{y}_k)^\top \tag{14}$$

where R_k is the covariance matrix of the measurement noise v_k.

• Correction: the weights are updated according to the likelihood $g_k(x_k)$, the transition density $p(x_k|x_{k-1})$ and the proposal density $q_k(x_k|x_{k-1}, y_k)$.

$$w_k^i \propto w_{k-1}^i \frac{g_k(x_k^i)p(x_k^i|x_{k-1}^i)}{\mathcal{N}(x_k^i; \bar{\mu}_k^i, \hat{P}_k)} \tag{15}$$

and $\sum_{i=1}^N w_k^i = 1$.

• Resampling: the particles x_k^i with high normalized weights w_k^i are selected and low-weighted particles are discarded. The selected particles are duplicated according to their weights in order to keep a constant total number of particles. The new set of particles is called x_k^i and the weights are set such that $w_k^i = 1/N$.

The resampling is used to decrease the weight variance and avoids degeneracy (i.e. when a single weight tends to unity and all the others tend to zero). See [8] or [9] for a survey on resampling methods. In practice, resampling is triggered by monitoring a criterion, such as the approximate efficiency [10], [11]:

$$N_{\mathit{eff},k} = \frac{1}{\sum_{i=1}^N \left(w_k^i\right)^2} \tag{16}$$

Resample is triggered whenever $N_{\mathit{eff},k} < N_{\text{th}}$ where N_{th} is a given threshold.

C. Monte Carlo filters performance criterion

The performance of Monte Carlo approaches can be evaluated by the asymptotic variance of the unnormalized weights given by [12], $\forall\ i = 1, \ldots, N$:

$$\mathbb{V}\text{ar}(\tilde{w}_k^i) = \frac{1}{N}\left(\frac{\int \frac{g_k(x_k)^2 p_{k|k-1}(x_k)^2}{q_k(x_k)} dx_k}{\left(\int g_k(x_k) p_{k|k-1}(x_k) dx_k\right)^2} - 1\right) \tag{17}$$

where the proposal density $q_k(x_k|x_{k-1}, y_k)$ is simplified as $q_k(x_k)$. When this variance is small, the Monte Carlo filter estimate is accurate, which reduces degeneracy phenomena.

III. Interacting Weighted Ensemble Kalman Filter

In this section, we introduce the Interacting Weighted Ensemble Kalman Filter (IWEnKF). We first determine a condition on the proposal covariance matrix so that it guarantees that the asymptotic variance of the unnormalized weights is finite (Section III-A). Guaranteeing a finite variance of the unnormalized weights provides an accurate Monte Carlo estimate. We then derive an analytic formulation of the IWEnKF that satisfies this condition (Section III-B).

A. Upper bound of the asymptotic variance of the unnormalized weights

Thereafter, the prior $p_{k|k-1}(x_k)$ and the proposal $q_k(x_k)$ densities are considered Gaussian. The mean of the prior density is $\tilde{x}_k$ and the covariance matrix is $\tilde{P}_k$, such that:

$$p_{k|k-1}(x_k) \propto \exp\left(-\frac{1}{2}\ (x_k - \tilde{x}_k)^\top \tilde{P}_k^{-1}(x_k - \tilde{x}_k)\right) \tag{18}$$

The expression of the proposal density is similar to (18), where $\tilde{x}_k$ is replaced by $\hat{x}_k$ and $\tilde{P}_k$ by $\hat{P}_k$.

Under these Gaussian assumptions, we state in Proposition 1 that the asymptotic variance admits a finite upper bound under a condition on the proposal covariance matrix $\hat{P}_k$.

Proposition 1: Assume that the prior $p_{k|k-1}(x_k)$ and the proposal densities $q_k(x_k)$ are Gaussian with covariance matrices $\tilde{P}_k$ and $\hat{P}_k$ respectively. If $\hat{P}_k - \tilde{P}_k$ is positive definite then the asymptotic variance of the unnormalized weights is finite:

$$\hat{P}_k - \tilde{P}_k > 0 \Leftrightarrow \mathbb{V}\text{ar}(\tilde{w}_k^i) < +\infty \tag{19}$$

Proof: The asymptotic variance of the unnormalized weights (17) is bounded if:

$$\int \frac{g_k(x_k)^2 p_{k|k-1}(x_k)^2}{q_k(x_k)} dx_k < +\infty \tag{20}$$

By taking the supremum, it comes:

$$\int \frac{g_k(x_k)^2 p_{k|k-1}(x_k)^2}{q_k(x_k)} dx_k \leq \sup_{x_k \in \mathbb{R}^d} g_k(x_k) \sup_{x_k \in \mathbb{R}^d}\left(\frac{p_{k|k-1}(x_k)}{q_k(x_k)}\right) \int g_k(x_k) p_{k|k-1}(x_k) dx_k \tag{21}$$

We assume that the likelihood $g_k(x_k)$ is bounded.

Thus a sufficient condition for the asymptotic variance of the unnormalized weights to be bounded is:

$$\sup_{x_k \in \mathbb{R}^d}\left(\frac{p_{k|k-1}(x_k)}{q_k(x_k)}\right) < +\infty \tag{22}$$

Equation (22) is equivalent to $\log\left(\frac{p_{k|k-1}(x_k)}{q_k(x_k)}\right) < +\infty$. By replacing the densities $p_{k|k-1}(x_k)$ and $q_k(x_k)$ by their expressions (18), it follows:

$$\log\left(\frac{p_{k|k-1}(x_k)}{q_k(x_k)}\right) \propto \frac{1}{2}(x_k - \hat{x}_k)^\top \hat{P}_k^{-1}(x_k - \hat{x}_k) - \frac{1}{2}(x_k - \tilde{x}_k)^\top \tilde{P}_k^{-1}(x_k - \tilde{x}_k) \tag{23}$$

By simultaneously adding and subtracting $\tilde{x}_k$ and pooling the terms, the logarithm (23) can be written as follows:

$$\log\left(\frac{p_{k|k-1}(x_k)}{q_k(x_k)}\right) \propto -\frac{1}{2} X_k^\top \left(\tilde{P}_k^{-1} - \hat{P}_k^{-1}\right) X_k + V_k^\top X_k \tag{24}$$

where $V_k = \hat{P}_k^{-1}(\tilde{x}_k - \hat{x}_k)$ and $X_k = (x_k - \tilde{x}_k)$.

It comes:

$$\lim_{||X_k|| \to +\infty} \log\left(\frac{p_{k|k-1}(x_k)}{q_k(x_k)}\right) = -\infty \quad \text{if} \quad \tilde{P}_k^{-1} - \hat{P}_k^{-1} > 0 \tag{25}$$

which is equivalent to:

$$\sup_{x_k \in \mathbb{R}^d}\left(\frac{p_{k|k-1}(x_k)}{q_k(x_k)}\right) < +\infty \quad \text{if} \quad \hat{P}_k - \tilde{P}_k > 0. \tag{26}$$

■

In order to satisfy (19), the proposal covariance matrix $\hat{P}_k$ must be appropriately chosen. In the following section, we introduce a method to determine $\hat{P}_k$ in the WEnKF framework which leads to the IWEnKF formulation.

B. Interacting WEnKF

In practice, the proposal density given by the WEnKF is the Gaussian given by (6). The proposal covariance matrix $\hat{P}_k$ is not guaranteed to satisfy the conditions of Proposition 1 ($\hat{P}_k - \tilde{P}_k > 0$). Thus, $\hat{P}_k$ can be replaced with a new covariance matrix $\hat{P}_k^*$ so that $\hat{P}_k^* - \tilde{P}_k > 0$ by slightly enlarging the proposal covariance matrix $\hat{P}_k$. This approach allows a greater overlap between the proposal density and the posterior density as illustrated in Fig 1.

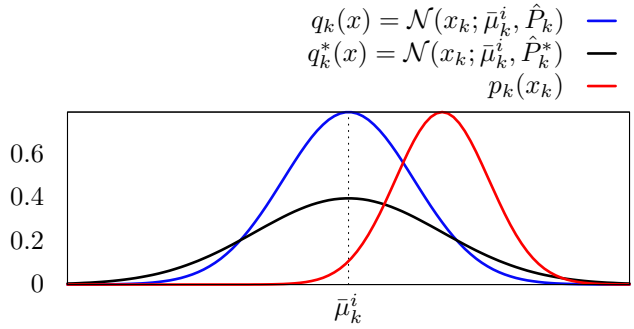

Fig. 1: Scheme of the overlaps between the posterior density (red curve), the original WEnKF proposal density ((6), blue curve), and the proposal density with a larger covariance matrix ((27), black curve).

Proposition 2: A proposal covariance matrix $\hat{P}_k^*$ that satisfies the condition of Proposition 1 i.e. $\hat{P}_k^* - \tilde{P}_k > 0$, is:

$$\hat{P}_k^* = \frac{1}{2}(\hat{P}_k + \tilde{P}_k + H_k) \tag{27}$$

where:

- $\hat{P}_k$ is the Kalman updated covariance matrix (8);
- $\tilde{P}_k$ is the prior covariance matrix (18);
- H_k is obtained from the polar decomposition of $\hat{P}_k - \tilde{P}_k$.

Proof: Solving $\hat{P}_k - \tilde{P}_k > 0$ is equivalent to finding a symmetrical matrix P_k solution of the following constrained optimization problem:

$$\min_{P_k - \tilde{P}_k > 0} ||P_k - \hat{P}_k||_F^2 \tag{28}$$

where $||.||_F$ is the Frobenius norm. In order to keep the information contained in the initial covariance matrix of the proposal density, we want to find P_k close to $\hat{P}_k$.

By simultaneously adding and subtracting $\tilde{P}_k$ in (28), it comes:

$$\min_{P_k - \tilde{P}_k > 0} ||P_k - \tilde{P}_k - (\hat{P}_k - \tilde{P}_k)||_F^2 \tag{29}$$

By taking $V_k = P_k - \tilde{P}_k$ and $A_k = \hat{P}_k - \tilde{P}_k$, it follows:

$$\min_{V_k > 0} ||V_k - A_k||_F^2 \tag{30}$$

The solution according to Higham's theorem [13] is:

$$V_k^F = \frac{1}{2}(A_k + H_k) \tag{31}$$

where H_k is obtained from the polar decomposition of $\hat{P}_k - \tilde{P}_k$, i.e. $\hat{P}_k - \tilde{P}_k = U_k H_k$ with $U_k^\top U_k = \mathbf{I}_d$ where $\mathbf{I}_d$ is the identity matrix of dimension d. The solution of the optimization problem (28) is thus:

$$\hat{P}_k^* = V_k^F + \tilde{P}_k = \frac{1}{2}(\hat{P}_k + \tilde{P}_k + H_k) \tag{32}$$

■

Proposition 2 introduces a new proposal covariance matrix for the IWEnKF that satisfies the conditions of Proposition 1. As a result, IWEnKF guarantees that the asymptotic variance of the unnormalized weights is finite. The new proposal covariance matrix is obtained via a polar decomposition which can be polynomially computed [14]. In practice, this is likely to bring more robustness to nonlinearities and multimodality.

The algorithm of IWEnKF is described in Algorithm 1.

Algorithm 1 Interacting WEnKF

Initialization: For $i = 1, \ldots, N$, initialize the particles $x_0^i \sim p_0$ from a prior distribution and set $w_0^i = 1/N$.
for k = 1,2,... **do**
- [Prediction:] For all particles, compute the mean and the covariance matrix of the proposal density (6). Compute $\hat{P}_k^*$ using (27) and sample x_k^i from the new proposal density $\mathcal{N}(x_k; \bar{\mu}_k^i, \hat{P}_k^*)$.
- [Correction:] $\forall i$, update and normalize the weights: $\tilde{w}_k^i \propto w_{k-1}^i \frac{g_k(x_k^i) p_{k|k-1}(x_k^i | x_{k-1}^i)}{\mathcal{N}(x_k^i; \bar{\mu}_k^i, \hat{P}_k^*)}$; $w_k^i = \tilde{w}_k^i / \sum_i \tilde{w}_k^i$.
- [Estimation:] compute the filter estimate $\hat{x}_k = \sum_i w_k^i x_k^i$ and the associated covariance matrix $\hat{P}_k = \sum_i w_k^i (x_k^i - \hat{x}_k)(x_k^i - \hat{x}_k)^\top$.
- [Resampling:]

if $N_{eff,k} < N_{\text{th}}$ **then**
Apply some resampling procedure as described at the end of Section II-B.
end if
end for

IV. Simulation Example

To illustrate the behavior of the proposed IWEnKF filter, it will be compared with the standard WEnKF on an underwater TAN example. Comparisons are done with the metrics described in Section IV-C.

A. Underwater TAN

Underwater TAN provides a drift-free navigation method for UUVs while avoiding resurfacing for a GPS update. The availability of seabed maps as well as the emergence of precise telemeters make the method suitable for underwater navigation. TAN [3] aims to retrieve the vehicle current state (e.g. position, velocity) by matching a terrain profile obtained from a sensor with a profile reconstructed from an embedded map of the operation area.

We consider an UUV equipped with a multi-beam telemeter and an embedded map of the area of operation shown in Fig 2. The reference trajectory is located in an ambiguous area of the map (see Fig 3). The spatial resolution of the map is about 100 meters. Measurements and predicted measurements of the filters are obtained by bilinear interpolations.

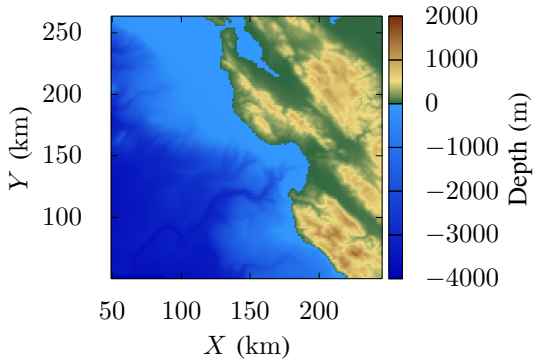

Fig. 2: Bathymetric map of the California coast (35°51′ N, 121°27′ W). The colorbar represents the depth levels (m).

B. State-space model

Let us consider a simplified navigation model. The vehicle state x is comprised of the position p and the velocity v, where $p = [p^x, p^y, p^z]^\top$ is expressed in meter and $v = [v^x, v^y, v^z]^\top$ is expressed in meter per second. The state equation is written in the following discrete way:

$$x_k = \begin{bmatrix} p_k \\ v_k \end{bmatrix} = \begin{pmatrix} \mathbf{I}_3 & \Delta_k\, \mathbf{I}_3 \\ \mathbf{0}_3 & \mathbf{I}_3 \end{pmatrix} x_{k-1} + \eta_k \tag{33}$$

where $\mathbf{I}_3$ and $\mathbf{0}_3$ are respectively the identity matrix and the zeros matrix of dimension 3 by 3, Δ_k is the discretization time-step and η_k a Gaussian process noise i.i.d. of covariance matrix Q. η_k represents the uncertainty of the model.

The measurement is made up of m beams: $y = [r_1, \ldots, r_m]^\top$. Each measurement r_i records the distance between the UUV and the seabed. The measurement equation is constructed via a projection in the Cartesian coordinate system (see Meduna [2] for details). For $i = 1, \ldots, m$,

$$r_i = \sqrt{(p^x - p_i^x)^2 + (p^y - p_i^y)^2 + (p^z - \text{map}_{\text{mb}}(p_i^x, p_i^y))^2} + v_i \tag{34}$$

where map_{mb} is the seabed depth of the operation area and v_i the measurement noise with R its covariance matrix. The map is a function of $\mathbb{R}^2$ in $\mathbb{R}$, taking as input the position in axis x and y and giving as output the elevation of the terrain.The range r_i is computed by determining $p_i = [p_i^x, p_i^y, p_i^z]^\top$ with $p_i^z = \text{map}_{\text{mb}}(p_i^x, p_i^y)$, the intersection point of the inertial beam direction vector with the terrain (see Fig 3.4 in [2]). As the intersection point is unknown in practice, the multi-beam telemeter measurement equation (34) is computed through numerical approximations (here via grid search method). The measurement noise takes these approximations into account in addition to sensor and map errors.

C. Comparison criteria

Comparisons are done by using the following criteria, evaluated for $N_{mc} \in \mathbb{N}^*$ Monte Carlo simulations.

- The Root Mean Square Error (RMSE) of filters:

$$\text{RMSE}_k^x = \sqrt{\frac{\sum_{i=1}^{N_{mc}} ||\hat{x}_k^i - x_k||_2^2}{N_{mc}}} \tag{35}$$

where $\hat{x}_k^i$ is the state estimate for the i^{th} Monte Carlo simulation. We will compare the RMSE with an approximation of the Posterior Cramér Rao Bound (PCRB) which is calculated according to the Tichavský recursive formula [15]. PCRB is approximated over 300 state samples at each time-step.

- The number of non-convergences:
The filter is said to not converge if, at the end of the trajectory, during the last 5 consecutive measurement time-steps, the state estimate $\hat{x}_k$ leaves the confidence ellipsoid Γ_k given by the PCRB, such that

$$\Gamma_k = \left\{ x_k | (x_k - \hat{x}_k)^T PCRB_k^{-1} (x_k - \hat{x}_k) \leq \alpha_{\text{th}}^2 \right\} \tag{36}$$

where the threshold α_{th} is such that $\mathbb{P}(\mathcal{X}^2(d) \leq \alpha_{\text{th}}^2) = 0.99$ with d the dimension of the state vector and $\mathcal{X}^2$ the Chi-squared distribution.

D. Simulation and results

Scenario parameters

- Number of Monte Carlo simulations: 50
- Sampling period: $\Delta_k = 5$ s
- Number of bathymetric measurements: 420
- Trajectory duration: 35 min
- Number of beams: $m = 5$
- Resampling threshold: $N_{\text{th}} = 0.75\ N$
- Standard deviation of each beam range: $\sigma_R = 10$ m

The initial uncertainty of the position is set to $P_0^p = diag([1000, 1000, 100]^2)$ and that of the velocity is set to $P_0^v = diag([0.5, 0.5, 0.5]^2)$. The notation $diag([A])$ is the matrix with the elements of A in the diagonal and 0 elsewhere. The initial state is $x_0 = [110000, 140000, -100, 5, 5, 0.05]^\top$. The standard deviation of the process noise is $Q = diag([3, 3, 3.10^{-1}, 2.10^{-2}, 2.10^{-2}, 2.10^{-3}]^2)$.

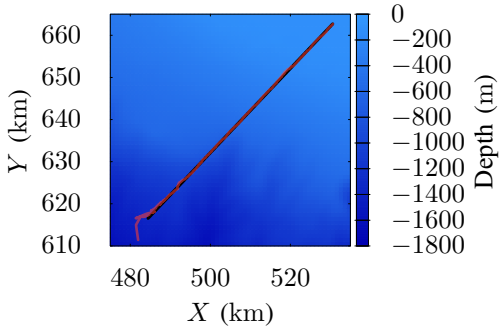

Fig. 3: Bathymetric map of the California coast with the true trajectory (black line) and the trajectory estimated by IWEnKF (red line).

The number of particles is $N = 3000$ for both filters. The initial errors and the measurements realizations are also shared. For one Monte Carlo simulation, Fig 3 illustrates the quick convergence of a IWEnKF trajectory towards the true trajectory.

Fig 4 shows the RMSEs for both filters using the simulation conditions described above. The RMSE of the horizontal position is calculated as follows:

$$\text{RMSE}_k^{p_h} = \sqrt{\text{RMSE}_k^{p^x\,2} + \text{RMSE}_k^{p^y\,2}} \tag{37}$$

The horizontal velocity is computed as above by replacing p_k by v_k, p^x by v^x and p^y by v^y.

Note that the RMSE curves can be lower than the PCRB curve at some point because PCRB is obtained by recursive approximation [15]. Only convergent Monte Carlo simulations are used to plot the curves on Fig 4. The non-convergence percentage is provided in Fig 5.

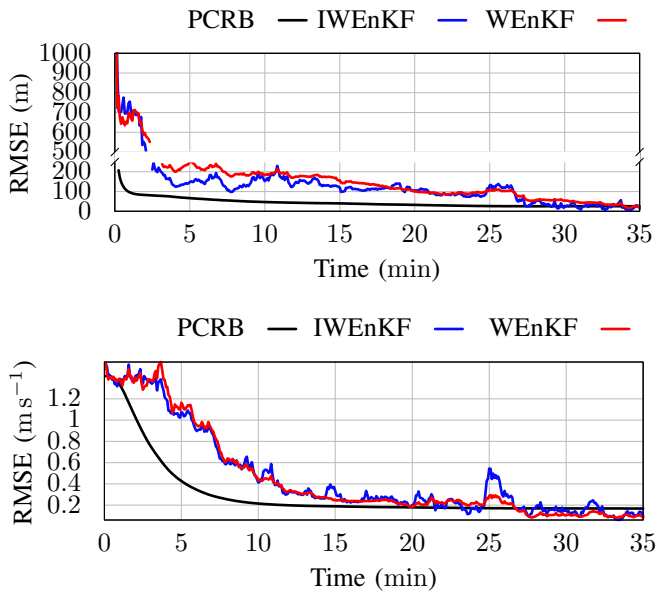

Fig. 4: Plot of PCRB and RMSEs for the horizontal position (upper plot) and for the horizontal velocity (lower plot).

The curves follow the tendency of the PCRB. Position and velocity RMSEs decrease with time and converge to a value close to the PCRB approximation.

Although the accuracy of the filter estimates is similar after 20 min of trajectory, the IWEnKF converges faster than the WEnKF. Before the convergence of the filters (from 90 s, when the IWEnKF curve falls below the WEnKF curve, until 15 min), the average distance between the two curves is about 50 m for the horizontal position.

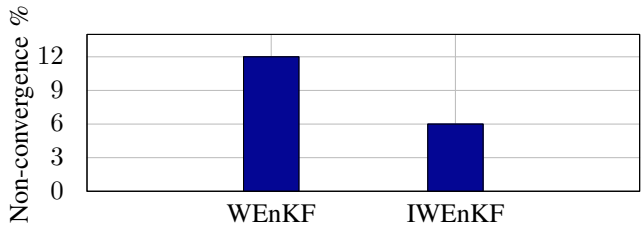

Fig. 5: Histogram of non-convergence percentage for 50 Monte Carlo simulations.

For 50 Monte Carlo simulations, the number of non-convergences is shown in Fig 5. The number of non-convergences of IWEnKF is twice as small as the one of WEnKF. This significant decrease in the number of non-convergences was expected as the IWEnKF method guarantees a bounded variance of the weights and thus prevents weight degeneracy.

V. Conclusion

This paper focuses on the Interacting Weighted Ensemble Kalman Filter (IWEnKF), an improved version of the Weighted Ensemble Kalman Filter. The proposed approach guarantees that the variance of weights remains bounded, which brings more robustness to nonlinearities in practice. IWEnKF was tested on an underwater Terrain Aided Navigation example. We demonstrated that IWEnKF is more robust to nonlinearities and measurement ambiguities than the classic version of the algorithm, as the number of non-convergences is significantly reduced. The guarantee of non-divergence of the variance of the weights will make it possible to embed this type of algorithm on autonomous systems such as UUVs.

References

[1] C. Palmier, K. Dahia, N. Merlinge, P. Del Moral, D. Laneuville and C. Musso. "Adaptive Approximate Bayesian Computational Particle Filters for Underwater Terrain Aided Navigation". In: *22nd International Conference on Information Fusion*. 2019.

[2] D. K. Meduna. "Terrain relative navigation for sensor-limited systems with application to underwater vehicles". In: *Stanford University*. 2011.

[3] J. Melo and A. Matos. "Survey on advances on terrain based navigation for autonomous underwater vehicles". In: *Ocean Engineering*. Vol.139, 2017, pp. 250-264.

[4] B.D.O. Anderson and J.B. Moore. "Optimal filtering". Prentice Hall, Englewood Cliffs, N.J. USA, 1979.

[5] P. Del Moral. "Nonlinear Filtering: Interacting Particle Resolution". In: *Markov Processes and Related Fields*. Vol.2, no.4, 1996, pp. 555-580.

[6] N. Papadakis, E. Mémin, A. Cuzol and N. Gengembre. "Data assimilation with the weighted ensemble Kalman filter". In: *Tellus A: Dynamic Meteorology and Oceanography*. Vol.62, 2010, pp. 673-697.

[7] M. Morzfeld, D. Hodyss and C. Snyder. "What the collapse of the ensemble Kalman filter tells us about particle filters". In: *Tellus A: Dynamic Meteorology and Oceanography*. Vol.69, no.1, 2017, pp. 1283809.

[8] T. Li, M. Bolic and P.M. Petar. "Resampling methods for particle filtering: classification, implementation, and strategies". In: *IEEE Signal processing magazine*. Vol.32, no.3, 2015, pp. 70-86.

[9] P. Del Moral, A. Doucet and A. Jasra. "On Adaptive Resampling Procedures for Sequential Monte Carlo Methods". In: *Bernoulli*. Vol.18, no.1, 2012, pp. 252-278.

[10] A. Kong, J.S. Liu and W.H. Wong. "Sequential imputations and Bayesian missing data problems". In: *Journal of the American statistical association*. Vol.89, no.425, 1994, pp. 278-288.

[11] A. Doucet, S. Godsill and C. Andrieu. "On sequential Monte Carlo sampling methods for Bayesian filtering". In: *Statistics and computing, Springer*. Vol.10, no.3, 2000, pp. 197-208.

[12] P. Del Moral. "Feynman-Kac formulae: Genealogical and interacting particle systems with applications, Probability and its applications". In: *Springer, New York*. 2004, pp. 25-32.

[13] N. J. Higham. "Computing a nearest symmetric positive semidefinite matrix". In: *Linear algebra and its applications*. 1988, pp. 103:103-118.

[14] N. J. Higham. "Computing the polar decomposition with applications". In: *SIAM Journal on Scientific and Statistical Computing*. Vol.7, no.4, 1986, pp. 1160-1174.

[15] P. Tichavsky, C.H. Muravchik and A. Nehorai. "Posterior Cramér-Rao bounds for discrete-time nonlinear filtering". In: *IEEE Transactions on signal processing*. Vol.46, no.5, 1998, pp. 1386-1396.